

Biologically-inspired selective filters

by

Laura K. Maguire

B.S., Harvey Mudd College, 2013

A thesis submitted to the
Faculty of the Graduate School of the
University of Colorado in partial fulfillment
of the requirements for the degree of
Doctor of Philosophy
Department of Physics
2019

This thesis entitled:
Biologically-inspired selective filters
written by Laura K. Maguire
has been approved for the Department of Physics

Assistant Professor Loren Hough

Professor Meredith Betterton

Date _____

The final copy of this thesis has been examined by the signatories, and we find that both the content and the form meet acceptable presentation standards of scholarly work in the above mentioned discipline.

Maguire, Laura K. (Ph.D., Physics)

Biologically-inspired selective filters

Thesis directed by Assistant Professor Loren Hough

Placeholder text for abstract.

Dedication

Nice dedication goes here.

Acknowledgements

Loren Hough Meredith Betterton Matt Glaser Noel Clark Franck Vernery
Kathryn Wall Eric Verbeke Nate Crossette Katie Rainey Scott Tilden Sophie Reskin Elena
Arroyo Taylor Moon Lu ??? Andrea Egan Nick Bax
Allison Holt Nabanita Das Jeffre Allen
Mike Stefferson Stephanie Bryant Sadhana Sharma Christopher Bowman Danielle Konetski
Benjamin Fairbanks Joseph Dragavon

Contents

Chapter

1	Bound diffusion measurements	1
1.1	Experimental parameters	1
1.1.1	Nup contour length and valency	2
1.1.2	Binding affinity of NTF2 and FSFG	2
1.1.3	Quantifying concentration of tethered Nups	4
1.1.4	Free diffusion constant	5
1.2	Experimental procedures	5
1.2.1	Hydrogel preparation	6
1.2.2	Influx of transport factor and inert protein	7
1.2.3	Fluorescence recovery after photobleaching	7
1.3	Steady-state hydrogel properties	9
1.3.1	Gel dimension estimates	11
1.3.2	Partition coefficients and fraction of time spent bound	12
1.3.3	Bound-diffusion calculation	13
1.4	Influx analysis	14
1.4.1	Profile analysis	15
1.4.2	Accumulation analysis	16
1.5	FRAP analysis	18
1.5.1	Accounting for photobleaching	18

1.5.2	No-exchange solution to diffusion equation	19
1.5.3	Fourier transform solution to diffusion equation	20
1.6	Results	28
1.7	Discussion	31
	Bibliography	32
	Appendix	
A	Hydrogel nuclear pore mimic dataset	33

Tables

Table

Figures

Figure

1.1	Isothermal calorimetry titration curve: heat of injection vs. molar ratio of FSFG to NTF2. Fits are questionable but multiple runs suggest $K_D \approx 200 \mu\text{M}$	3
1.2	Influx image series. A hydrogel containing a nominal 5 mg/mL FSFG concat-2 was challenged with 20 μM NTF2-F and mCherry. The hydrogel shows selective entry of NTF2-F and has largely equilibrated within 24 hours.	8
1.3	FRAP image series. NTF2-FITC (top, green) and mCherry (bottom, red) bleaching and recovery shown separately. Hydrogel contained...	10
1.4	Sample hydrogel mask with radius and center calculations. (A) An equilibrated hydrogel containing FSFG concat-1, immediately post-bleach. (B) The corresponding hydrogel mask (white), bleach spot mask (light gray), calculated gel diameter, and calculated gel center.	11
1.5	Partitioning of NTF2 and mCherry into FSFG hydrogel. (A) Partition coefficient γ depends on whether the hydrogel excludes or binds protein. (B) Equilibrated FSFG concat-1 hydrogel (nominally 10 mg/mL) showing partitioning of $T_L = 20 \mu\text{M}$ each NTF2-FITC and mCherry. Contrast adjusted for ease of viewing.	12

1.6	Intensity profiles and total accumulation within hydrogel as determined from influx time series. (A) Image of an FSFG concat-2 hydrogel with a nominal Nup concentration of 10 mg/mL. Reservoir contains 20 μ M NTF2-F and mCherry in PTB. Reservoir mask is shown (red polygon) as well as accumulation area and rectangle over which the profile averaging was performed. (B) Normalized intensity profiles as calculated using the box in (A). (C) Normalized average intensity within hydrogel.	14
1.7	Geometry used to solve diffusion equation in [3]. The reservoir concentration c_0 fixed the concentration at the edge of the region Ω . The concentration $c(\mathbf{r}, t)$ is determined within Ω as a function of position and time.	15
1.8	Fits to Eqn. 1.8 near the beginning of the influx experiment for (A) mCherry and (B) NTF2-Alexa488 intensity profiles. Hydrogel nominally contains 10 mg/mL FSFG-PEGDA 700 kDa. The entire intensity profile is shown in the top panel with the portion used for fitting highlighted in red. Approximate locations of the gel edge, background fluorescence level, and partition coefficient are also shown.	17
1.9	Fits to Eqn. 1.8 at a fixed point near the gel edge for (A) mCherry and (B) NTF2-Alexa488 intensity profiles. The short-time approximation likely only holds for times $t \lesssim 20$ minutes. Hydrogel nominally contains 10 mg/mL FSFG-PEGDA 700 kDa.	17
1.10	Accumulation fits to Eqn. 1.10 for (A) mCherry and (B) NTF2-Alexa488. Hydrogel nominally contains 10 mg/mL FSFG-PEGDA 700 kDa.	18
1.11	Geometry for diffusion-equation solution Eqn. 1.13. A circle of radius a is centered at the origin. The boundary $r = a$ is held at concentration $c = 0$ and the interior has initial concentration profile $f(r, \theta)$	21
1.12	Reconstruction of initial concentration distribution. Reservoir is masked and not included. (A) Heatmap of original image with average equilibrated gel intensity set to zero. (B) Reconstruction using two Bessel orders ($N_\nu = 2$) and two zeros ($N_\alpha = 2$) in each order. (C-E) Reconstructions with $N_\nu = N_\alpha = 4, 10$, and 20	26

1.13 Heatmap of cosine and sine mode coefficients $C_{\nu,\alpha}$ and $S_{\nu,\alpha}$ for the reconstruction shown in Fig. 1.12E. Values are shown for each Bessel order ν and each zero α	26
1.14 Fits using the series expansion Eqn. 1.13. (A) NTF2-F and mCherry recovery curves for a no-nup hydrogel. (B) NTF2-F and mCherry recovery curves for a hydrogel nominally containing 10 mg/mL FSFG concat-1.	27
1.15 Bright NTF2-F ring surrounding photobleach spot, 70 minutes after bleaching. This ring often developed in FSFG concat-1 gels. Photobleach mask was chosen to be slightly smaller than the ring. Contrast adjusted for ease of viewing. While circle added to guide the eye.	28
1.16 (A) Partition coefficients for NTF2-F and mCherry in each of the three experimental conditions. (B) Fraction of NTF2-F bound as calculated using Sec. 1.3.2. All errors are standard error of the mean.	29
1.17 Recovery curves for (A) no-nup, (B) FSFG concat-1, and (C) FSFG concat-2 hydrogels. All curves are shown for both NTF2-F and mCherry. Dark lines are averaged curves. Pre-bleach intensity set to one.	30
1.18 (A) Observed diffusion constant for NTF2-F and mCherry in each of the three experimental conditions. (B) Calculated values of the bound diffusion constant D_B for NTF2-F in the FSFG hydrogels. All errors shown are standard error of the mean.	30
A.1 Parameters used to predict the bound diffusion constant for NTF2-F in FSFG hydrogels. Binding data is from [1].	33
A.2 Measured and calculated values for no-Nup hydrogels.	34
A.3 Measured and calculated values for FSFG concat-1 hydrogels, nominally containing 10 mg/mL FSFG.	34
A.4 Measured and calculated values for FSFG concat-2 hydrogels.	35

Chapter 1

Bound diffusion measurements

Following up on the principles of the bound-diffusion theory, we wanted to see whether we could measure bound diffusion in a biomaterial inspired by the nuclear pore complex. In order to do that, we made Nup-filled hydrogels and measured the diffusion of transport factors and inert proteins within them. We measured the diffusion in a few different ways: monitoring the concentration profile and total accumulation as the proteins diffused into the cell, and using fluorescence recovery after photobleaching (FRAP).

Fluorescence recovery after photobleaching (FRAP) relies on the redistribution of fluorophores after patterned photobleaching in order to determine their diffusion constant. After a small portion of the hydrogel is bleached, the bleached spot gradually exchanges with the non-bleached fluorophores outside, and the average fluorescence intensity within the bleached spot recovers. The recovery lifetime can be used to determine the fluorophore's diffusion constant, and the final recovered intensity as compared to the intensity outside the bleach spot can be used to determine the mobile fraction of fluorophore.

1.1 Experimental parameters

Our reaction-diffusion model of selectivity is controlled by a relatively small number of parameters. Ideally, we would like to vary all of these experimentally in order to verify the model's predictions. In reality, most are highly difficult to alter in a well-controlled way. Of the model's parameters, the contour length L_C of the tethered Nups is the simplest to control. Varying this

contour length will vary the bound diffusion coefficient D_B according to Eqn. ???. This section discusses L_C and the other experimental parameters used in our hydrogel nuclear pore mimics.

1.1.1 Nup contour length and valency

The most straightforward way to vary D_B is to change the contour length of the Nups that are anchored into the hydrogel. To that end, we compared hydrogels containing the constructs FSFG concat-1 and FSFG concat-2 (Sec. ??, Appendix ??). These Nup fragments have $L_C = 50$ nm and 100 nm, respectively. Given the parameters described below, the bound diffusion constant should increase by roughly 40% from FSFG concat-1 to FSFG concat-2.

In addition to differing lengths, the FSFG concat-1 and concat-2 differ in their number of binding sites, with six and twelve respectively. In order to control for the change in binding valency, we tested FSFG concat-2 hydrogels with the same molar concentration of FG repeats as the FSFG concat-1 gels as well as testing gels with the same molar concentration of Nups.

1.1.2 Binding affinity of NTF2 and FSFG

Although bound diffusion is the key parameter from our reaction-diffusion model of selectivity, the kinetic parameters of off-rate k_{off} , on rate k_{on} , and dissociation constant $K_D = k_{\text{off}}/k_{\text{on}}$ are also important. These parameters are surprisingly difficult to measure, yielding values between 10 nM and 10 μM depending on the experimental conditions. We estimated the dissociation constant for NTF2 and FSFG concat-1 using isothermal titration calorimetry (ITC). The heat of injection was recorded as FSFG was titrated into a stock of NTF2. While the resulting titration curves had low signal-to-noise and did not reach saturation, they clearly indicated binding (Fig. 1.1). Simple fits are likely inaccurate, given the high degree of multivalent binding, but may provide an order-of-magnitude estimate of the affinity. Several ITC curves agree on a dissociation constant of $K_D \approx 200\mu\text{M}$. This is roughly compatible with the millimolar per-FSFG constant measured by the Rout lab with NMR and ITC [1]. Similarly weak values were predicted through NMR, simulation, and stopped-flow anisotropy [2].

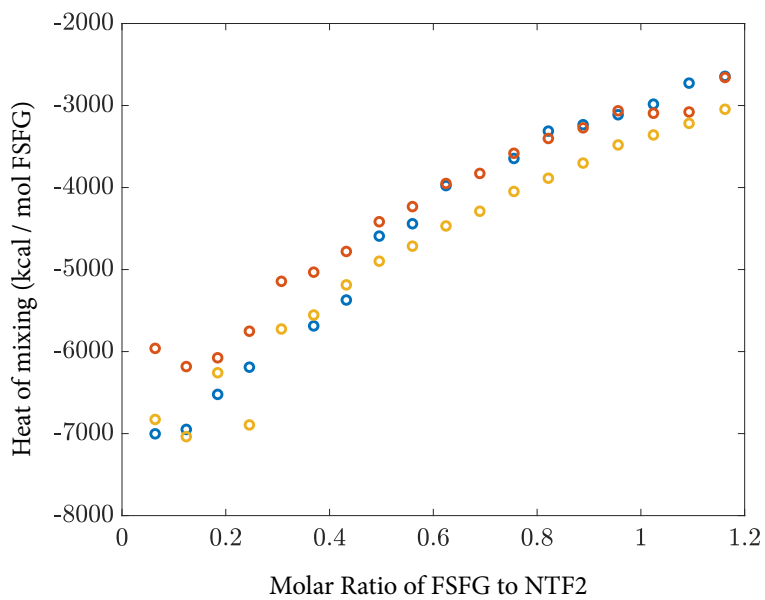


Figure 1.1: Isothermal calorimetry titration curve: heat of injection vs. molar ratio of FSFG to NTF2. Fits are questionable but multiple runs suggest $K_D \approx 200 \mu\text{M}$.

Due to the twin difficulties of varying K_D in a controlled way and accurately measuring its value, we did not attempt to experimentally alter this parameter. Ideally, a transport factor - Nup pair with $K_D \approx 1\mu\text{M}$ would have been used to maximize selectivity. For the purposes of determining the bound diffusion constant, the only value that is necessary to measure is the ratio K_D/N_T , which can be estimated using the partitioning of transport factors and inert proteins into the FSFG hydrogels (Sec. 1.3.2). We investigated using the ubiquitin-associated (UBA) domain of the mRNA exporter Mex67 as a Nup-binding domain in GFP fusion proteins. In principle, varying numbers of this small (<10 kDa) domain could be added to GFP to explore the effect of varying binding affinity and valency in transport factors. The constructs GFP-UBA, GFP-UBAx2, and GFP-UBAx3 were created by Eric Verbeke, but did not express and/or bind well.

1.1.3 Quantifying concentration of tethered Nups

Another potentially-tunable parameter of the bound-diffusion model is N_T , the total concentration of tethered Nups. It is straightforward to control the Nup concentration in the hydrogel precursor solution by resuspending a known mass of lyophilized protein. Nup concentrations up to ~ 50 mg/mL can be resuspended. However, it is much more difficult to determine how much protein was tethered to the hydrogel upon crosslinking.

BCA protein quantitation assays were used to place upper bounds on N_T . Two methods were attempted: incubating the hydrogel itself in the working reagent, and soaking the hydrogel in a known volume of buffer and testing the concentration of FSFG released. When applying the first method, the hydrogel was first soaked to remove excess precursor solution and thoroughly rinsed. The gel was placed into a 96-well plate and buffer added until the appropriate sample volume was reached. A standard BCA protocol was then followed. Upon incubation with the working reagent, the hydrogels turned purple, as expected. Standard absorption measurements and processing yielded an estimate of 0.5 mg/mL tethered FSFG-concat 1; this should be taken as an approximate value only. The second method, that of soaking hydrogels and measuring the FSFG released, placed a similarly-low upper bound on tethered FSFG concentration. Hydrogels

made with 5 μL of precursor solution were soaked in 45 μL buffer to equilibrate. The buffer was then measured to have a concentration of 1.0 mg/mL FSFG, implying a tethered FSFG concentration of < 1 mg/mL.

The concentration of Nups within the pore may reach 100 mg/mL [?]. The low concentration of tethered Nups that we were able to achieve is therefore a major barrier to selectivity. It is likely that the disordered nature of FSFG makes the labeled end less accessible to the hydrogel scaffold than would be the case for an ordered protein. In an effort to overcome this limitation, we tested other linkers and conjugation methods. We conjugated the FSFG-cys to PEG-diacrylate of varying lengths (700 Da and 10 kDa), to multi-armed PEG-diacrylate, and to maleimide-PEG-acrylate. While labeling was verified using Ellman's reagent (Appendix ??), there was no noticeable difference in transport factor partitioning into these hydrogels.

1.1.4 Free diffusion constant

The final tunable parameter from the binding-diffusion model is the diffusion constant of the transport factor when it is not bound to a Nup, the free diffusion constant D_F . Decreasing D_F is predicted to increase a material's selectivity while decreasing the absolute flux of transport factor (Figs. ??, ??). The free diffusion is predominantly determined by the protein's size and the viscosity of the solution, according to the Stokes-Einstein equation $D = k_B T / 6\pi\eta R$, where $k_B T$ is the thermal energy, η the solution viscosity, and R the particle radius. The solution viscosity could potentially be increased using a viscous additive such as glycerol; however, these attempts appeared to interfere with the binding of NTF2 and FSFG.

The diffusion of the non-binding 30 kDa protein mCherry was used as a proxy for the free diffusion of similarly-sized NTF2 within the FSFG hydrogels.

1.2 Experimental procedures

The nuclear pore mimics in this dataset were designed with the lessons of Chapter ?? in mind. They consist of hydrogels with the largest average pore size and simplest geometry: a single

microliter-scale droplet. While this geometry does not allow for direct measurements of selectivity, the in-gel diffusion constants of both NTF2 and mCherry can be determined and bound diffusion calculated. Two types of experiments were carried out: influx experiments, in which the entry of fluorescent proteins into the hydrogels was monitored, and FRAP experiments, in which a portion of an equilibrated hydrogel was bleached and the recovery observed. Both experiments provide a measurement of the proteins' diffusion constants. These experiments were performed at CU's BioFrontiers Advanced Light Microscopy Core Facility. Thanks go to Joseph Dragavon for much assistance with the microscopy.

1.2.1 Hydrogel preparation

Detailed precursor solution recipes are given in Appendix ???. For the dataset analyzed in this chapter, all nuclear pore mimic hydrogels were 6% acrylamide and contained 2 mM LAP. The precursor was made with potassium transport buffer (PTB) and contained either FSFG concat-1 bis or FSFG concat-2 bis. Lyophilized FSFG-bis was resuspended in PTB, allowed to sit at room temperature for at least 20 minutes, and added to the precursor solution. After the precursor solution was thoroughly mixed, it was degassed in a vacuum desiccator for 10 minutes and immediately pipetted into a disassembled 400- μm -thick PDMS gasket chamber (Sec. ??). Drops between 0.5 and 2 μL were carefully pipetted onto the plastic slide and the chamber assembled around the drops. Typically, each chamber measured a few centimeters on a side and contained a control gel with no Nups as well as one or more Nup-filled gels. The chamber was then illuminated as uniformly as possible with 365 nm light at approximately 200 mW/cm^2 with a ThorLabs M365 LP1 LED. Condensation around the gels indicated that they had crosslinked. The chamber was immediately rinsed with at least 100 μL of PTB, filled with fresh PTB, and sealed with a PDMS slab and clingwrap. The gels were left to soak at 4°C for at least 12 hours so that any remaining precursor solution and protein could leave the gel.

1.2.2 Influx of transport factor and inert protein

After soaking in buffer, the buffer solution was removed by pipette or wicking with a Kimwipe and a fluorescent reservoir solution added. Aspirating the chamber was avoided if possible, as it sometimes disturbed the seal between the gel and the chamber. The reservoir solution contained 20 μM each freshly-thawed NTF2-fluorescein (NTF2-F) and mCherry in PTB. The chamber was resealed after adding the solution. If no influx experiment was planned, the gels were then allowed to equilibrate for 24 hours before FRAP was performed.

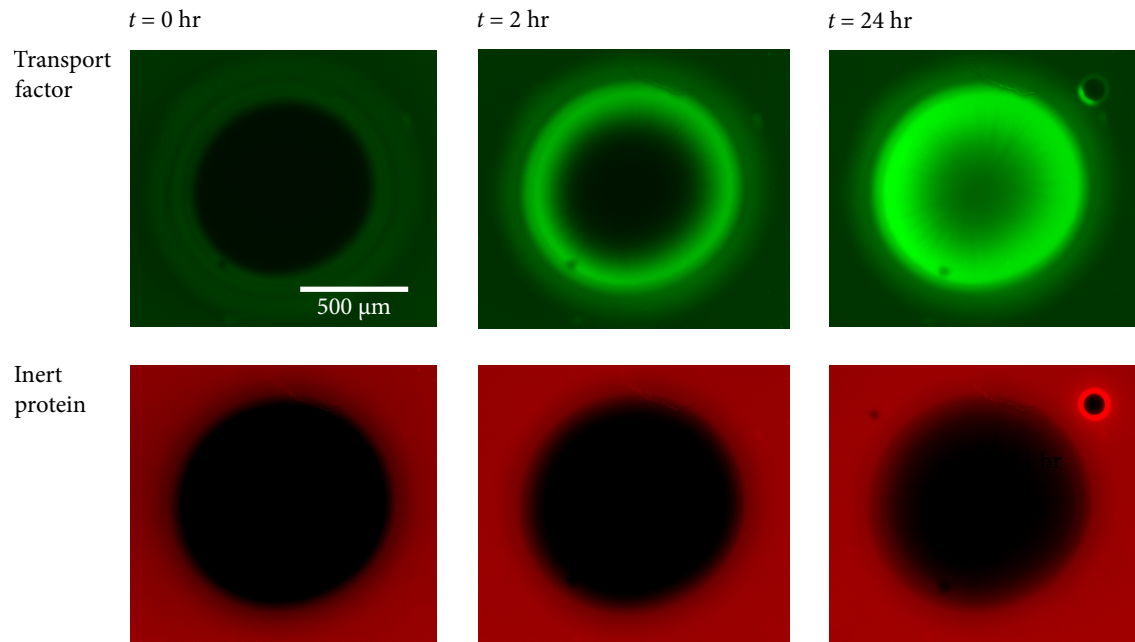
When influx experiments were run, they began as soon as possible after loading the reservoir solution. Videos were recorded at 4x magnification on an Olympus IX-81 widefield microscope using FITC (excitation 464-500 nm / emission 516-556 nm) and TRITC (excitation 532-544 nm / emission 573-613 nm) filter cubes. Exposure times were typically 30-100 ms with 3-8 dB gain. Videos consisted of 120 frames at one frame per minute. Minimal photobleaching took place over the course of these experiments. After the influx experiment, the chamber was usually stored for equilibration 4°C, protected from light, and a FRAP experiment performed the following day.

Influx experiments on hydrogels containing FSFG show binding of NTF2-F to mCherry (Fig. 1.2). A bright wavefront of NTF2-F slowly progresses into the gel, while mCherry remains largely excluded. As expected, mCherry equilibrates more rapidly than does NTF2-F, due to the lack of binding. Influx experiments were analyzed as described in Sec. 1.4.

1.2.3 Fluorescence recovery after photobleaching

FRAP is typically performed using a confocal microscope, but we were able to bleach the hydrogels using an Olympus IX-81 widefield microscope. The widefield was preferable because the greater depth of field allowed for thicker hydrogel samples, which were easier to fabricate and manipulate. As described above, the hydrogel was first allowed to equilibrate with 20 μM NTF2-F and mCherry in PTB. A reference image was taken at 4x magnification in both fluorescence channels. A circular region of the hydrogel around 300 μm (?? check this) in radius was then

Figure 1.2: Influx image series. A hydrogel containing a nominal 5 mg/mL FSFG concat-2 was challenged with 20 μ M NTF2-F and mCherry. The hydrogel shows selective entry of NTF2-F and has largely equilibrated within 24 hours.



photobleached by taking a five-second exposure at 40x magnification using a DAPI (excitation 352-402 nm / emission 417-477 nm) filter cube. Following the bleach, the 4x objective was rapidly returned and a time series recorded. Typical series consisted of 15-30 frames taken as rapidly as possible (5-10 s per frame), followed by 30-60 frames taken at a slower rate (1-2 minutes per frame). Total experiment time was 1-4 hours. Typical exposure times were 10 ms for NTF2-F and 40 ms for mCherry, both with a gain of 3 dB.

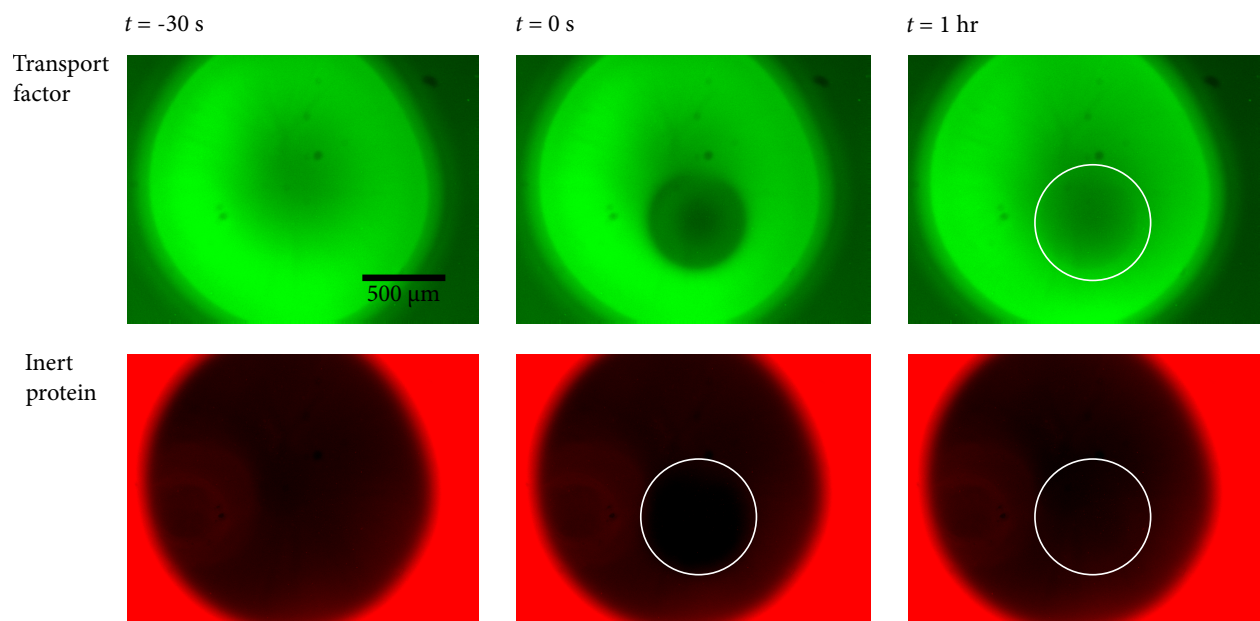
In order to increase throughput, up to three FRAP experiments were run concurrently by sequentially bleaching and then imaging several locations within a single chamber. This led to a maximum delay time of approximately 35 s between the end of the bleach segment and the beginning of the time series. Delay times were recorded and taken into account in the data processing. Figure 1.3 shows a representative series of images pre- and post-FRAP for both NTF2-F and mCherry.

Despite allowing 24 hours for equilibration, the fluorescence intensity across the hydrogel was not always uniform at the beginning of a FRAP experiment. This could be due to slow diffusion into the hydrogels, or to inhomogeneous crosslinking. The center of a hydrogel is more likely to be tightly crosslinked than the edges, as swelling is most inhibited at the center. Gels which were too inhomogenous to display a clear bleach spot were discarded, but many nonuniform hydrogels were used in the final dataset, with the lack of equilibrium addressed in the data analysis (Sec. 1.5). Smaller hydrogels ($0.5 \mu\text{L}$ of precursor solution) equilibrated more readily, at the cost of increasing the effect of fluorescent protein exchange with the reservoir, since the bleach spot then covered a significant fraction of the hydrogel. This effect was also taken into account during data analysis.

1.3 Steady-state hydrogel properties

Both the influx and FRAP experiments rely on steady-state properties of the hydrogel as well as time-dependent ones. These properties include the partition coefficients of transport factors and inert proteins, as well as some dependent on the geometry of the hydrogel.

Figure 1.3: FRAP image series. NTF2-FITC (top, green) and mCherry (bottom, red) bleaching and recovery shown separately. Hydrogel contained...



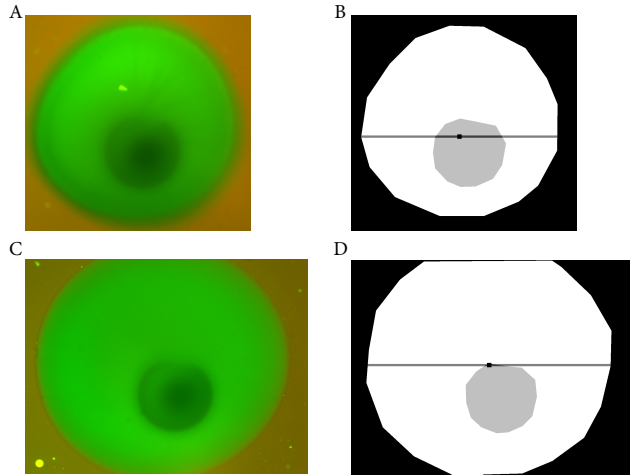


Figure 1.4: Sample hydrogel mask with radius and center calculations. (A) An equilibrated hydrogel containing FSFG concat-1, immediately post-bleach. (B) The corresponding hydrogel mask (white), bleach spot mask (light gray), calculated gel diameter, and calculated gel center.

1.3.1 Gel dimension estimates

Although the hydrogels were not perfectly circular, all analysis treated them as circular or nearly so. In total, the analysis made use of a gel's radius, center, perimeter, and area. I began by manually defining two masks: one that covered the entire gel, and one that covered only the bleach spot (Fig. 1.4). The gel area was calculated by summing all of the pixels in the gel mask and, where necessary, making use of the $1.58 \mu\text{m}$ per pixel scale of the Olympus 4x objective. The perimeter was calculated using Matlab's `bwperim` function, which takes a binary mask and returns a mask whose only nonzero entries are that mask's perimeter. Summing over these pixels and scaling provides the gel perimeter. It should be noted that in some cases the full area of the gel was not within the field of view. In these cases, sometimes the partial area in the field of view was used as the area estimate, and sometimes I embedded the gel image in a larger frame and estimated the remaining area when drawing the mask. Following sections indicate which method was used and the mathematical reasoning. However, all perimeter calculations were performed with the estimated full area.

The hydrogel radius was estimated taking the diameter to be the widest row of the gel mask. The widest row also set the y-coordinate of the gel center, with the x-coordinate calculated to be midway along the non-zero values for that row. As seen in Fig. 1.4, this is a quick and relatively crude method, but in almost all cases it works reasonably well. An advantage of this method is

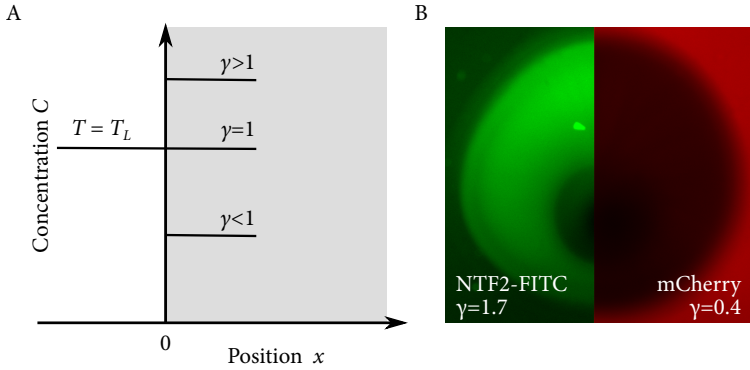


Figure 1.5: Partitioning of NTF2 and mCherry into FSFG hydrogel. (A) Partition coefficient γ depends on whether the hydrogel excludes or binds protein. (B) Equilibrated FSFG concat-1 hydrogel (nominally 10 mg/mL) showing partitioning of $T_L = 20 \mu\text{M}$ each NTF2-FITC and mCherry. Contrast adjusted for ease of viewing.

that it works even for hydrogels which do not fit in the vertical field of view.

1.3.2 Partition coefficients and fraction of time spent bound

The concentration of NTF2 and mCherry in a flow chamber's reservoir can be directly controlled, but the partitioning of a protein into the hydrogel depends on the degree to which the presence of the gel sterically excludes the protein, as well as on binding interactions between the gel and protein. When a transport-factor-sized inert protein is present to control for the steric effects, information about the transport factor's dissociation constant and fraction of time spent bound can be extracted from knowledge of the partition coefficient γ . In particular, p_B , the fraction of time spent bound, is necessary in order to calculate the bound diffusion coefficient.

As shown in Fig. 1.5A, the partition coefficient is the ratio of a protein's concentration in a well-equilibrated hydrogel to that in the surrounding reservoir. This quantity is calculated by dividing the average intensity of the gel by that of the reservoir within the field of view (Fig. 1.5B). If the gel is not fully equilibrated, the partition coefficient can be estimated using a line scan through the reservoir and gel, though this will likely underestimate the true value.

When the system is in chemical equilibrium, the concentration of free transport factor (T), free Nup (N), and transport factor - Nup complex (C) is related to the dissociation constant K_D by $K_D = NT/C \approx N_T T/C$ in the linear approximation $N \approx N_T$. The total tethered Nup concentration, both free and bound, is the constant N_T . The fraction of transport factors that are

bound is then given by

$$p_B = \frac{C}{C+T} = \frac{C}{C + \frac{CK_D}{N_T}} = \frac{1}{1 + \frac{K_D}{N_T}} \quad (1.1)$$

To relate this expression to measurable quantities, write the protein concentrations within the hydrogel in terms of their partition coefficients. The concentration c_0 of the inert protein and the transport factor is equal in the reservoir. If γ_T is the partition coefficient of the transport factor and γ_I that of the inert protein, then the transport factor concentrations can be expressed as

$$T = \gamma_I c_0 \quad (1.2)$$

$$C = T_T - T = \gamma_T c_0 - \gamma_I c_0 \quad (1.3)$$

The total transport factor concentration within the gel is $T_T = T + C$ and is a constant. Therefore, within the gel, the chemical equilibrium condition can be expressed as

$$\frac{K_D}{N_T} = \frac{T}{C} = \frac{\gamma_I c_0}{\gamma_T c_0 - \gamma_I c_0} = \frac{\gamma_I}{\gamma_T - \gamma_I} \quad (1.4)$$

Combining Eqns. 1.1 and 1.4, the bound probability can be expressed in terms of the partition coefficients as

$$p_B = \frac{1}{1 + \frac{K_D}{N_T}} = \frac{1}{1 + \frac{\gamma_I}{\gamma_T - \gamma_I}} = 1 - \frac{\gamma_I}{\gamma_T} \quad (1.5)$$

1.3.3 Bound-diffusion calculation

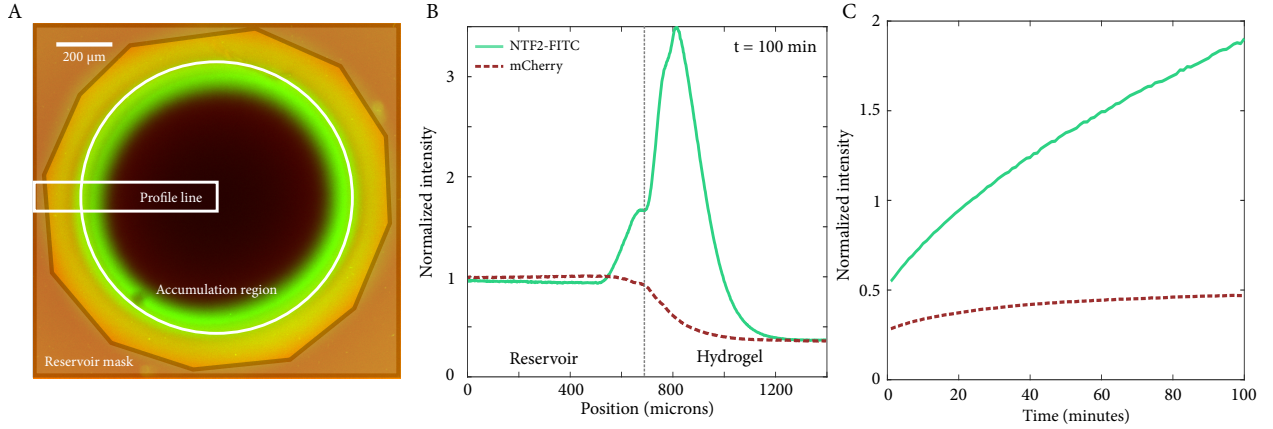
Once the observed diffusion constants for NTF2 and mCherry have been calculated, along with the fraction of time spent bound p_B , the bound diffusion is given straightforwardly by the weighted average

$$D_{\text{obs,TF}} = p_B D_B + (1 - p_B) D_F \quad (1.6)$$

This result assumes Fickian diffusion. In reality the diffusion will be slightly anomalous due to binding and the presence of the hydrogel. However, the binding is highly transient and the hydrogel relatively permeable to proteins of the size of NTF2 and mCherry (Sec. ??).

Taking the free diffusion coefficient of the transport factor to be approximately equal to the observed diffusion of the inert protein ($D_F = D_{\text{obs,I}}$), the bound diffusion coefficient of the transport

Figure 1.6: Intensity profiles and total accumulation within hydrogel as determined from influx time series. (A) Image of an FSFG concat-2 hydrogel with a nominal Nup concentration of 10 mg/mL. Reservoir contains 20 μ M NTF2-F and mCherry in PTB. Reservoir mask is shown (red polygon) as well as accumulation area and rectangle over which the profile averaging was performed. (B) Normalized intensity profiles as calculated using the box in (A). (C) Normalized average intensity within hydrogel.



factor is

$$D_B = \frac{D_{\text{obs,TF}} - (1 - p_B)D_{\text{obs,I}}}{p_B} \quad (1.7)$$

Note that neither the dissociation constant or the total Nup concentration need to be measured independently in order to calculate the bound diffusion constant.

1.4 Influx analysis

After recording a time series of fluorescent protein influx into a hydrogel, diffusion constants can be estimated using either a plot of the intensity profile across the gel or a plot of total accumulation within the gel. Figure 1.6 shows an example of each plot. The intensity within the gel is normalized to the average intensity of the reservoir, as calculated using the mask shown in Fig 1.6A. Therefore, each profile trace begins at $I = 1$ within the reservoir and either dips or rises to the partition coefficient value within the gel. As the gels are not equilibrated, much of the gel interior shows only background fluorescence. Likewise, the average intensity within the hydrogel trends towards the partition coefficient but does not reach it on the time scale of an average experiment.

Analysis of the accumulation and profile curves used the diffusion-equation solutions described

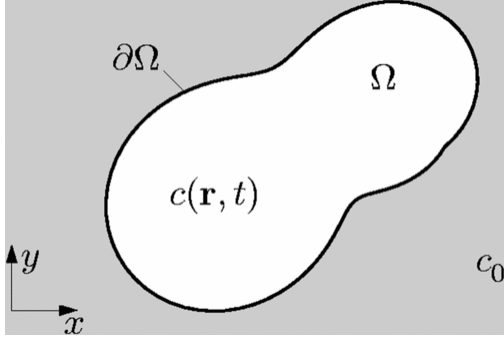


Figure 1.7: Geometry used to solve diffusion equation in [3]. The reservoir concentration c_0 fixed the concentration at the edge of the region Ω . The concentration $c(\mathbf{r}, t)$ is determined within Ω as a function of position and time.

by Mortensen, Okkels, and Bruus [3]. This method assumes that the edge of a nearly-circular two-dimensional region is held at a fixed concentration while the interior equilibrates (Fig. 1.7). Such boundary conditions correspond to an infinite fluorophore reservoir. Given that our reservoirs are 10-20 times larger than the hydrogel volume, this is a reasonable assumption. In a slight modification, we allow for an arbitrary partition coefficient γ by taking the fixed boundary concentration c_0 to be γT_0 , where T_0 is the fluorescent protein intensity in the reservoir. The assumption of near-circularity is also a good one.

The two most troublesome restrictions of the Mortensen equations are Fickian diffusion and the homogeneity of the hydrogel. As discussed in Sec. ??, the presence of the hydrogel meshwork and binding make diffusion within the hydrogels slightly anomalous. Additionally, despite the improvements to the fabrication protocol, the hydrogels likely contain some degree of nonuniformity in their density, with the centers most likely being slightly denser than the edges due to differential swelling. The effects of swelling and non-uniform thickness are greatest at the gel edge. Unfortunately, the points at the edge of the gel and earliest in the experiment are the most important to the following fits. As a result, the diffusion constants extracted using the profile and accumulation plots are not reliable. The analysis is presented below nonetheless, as a similar approach was taken in analyzing the FRAP experiments.

1.4.1 Profile analysis

Mortensen *et al* first define a characteristic timescale for equilibration $\tau = (\mathcal{A}/\mathcal{P})^2(\pi/4D)$ where \mathcal{A} and \mathcal{P} are the area and perimeter, respectively, of Ω . For a circle $\mathcal{A}/\mathcal{P} = a/2$, but this

ratio was numerically calculated for the hydrogels (Sec. 1.3.1). For times $t \ll \tau$, the concentration profile as a function of the distance r from the gel center can be approximated as

$$c(r, t) = c_0 \operatorname{erfc} \left(\frac{r}{\sqrt{4Dt}} \right) \quad (1.8)$$

where D is the diffusion constant.

The typical duration of an influx experiment was approximately τ , making the short-time approximation questionable throughout most of the time series. We attempted to fit the intensity profile (Fig. 1.8) and obtained fits with fairly low error but with unreliable fit parameters. In addition to the issues of timescale, it was often difficult to determine where the gel edge was located, as well as the partition coefficient. Given these problems, it is not surprising that fits at successive timepoints yielded incompatible values of diffusion constant for both mCherry and NTF2. A similar problem prevented the use of diffusion constants obtained from intensity fits at a fixed position over time (Fig. 1.9).

A more exact solution for $c(r, t)$ can be written if the gel is assumed to be circular. Mortensen *et al* quantify the error introduced by small deviations from circularity and find it to be small. Assuming a circular gel, the concentration profile at an arbitrary time t is given by

$$\frac{c(r, t)}{c_0} = 1 - 2 \sum_{n=0}^{\infty} \frac{J_0(\alpha_n r)}{\alpha_n a J_1(\alpha_n a)} \exp(-\alpha_n D t) \quad (1.9)$$

where a is the gel radius and $\alpha_n a$ is the n th zero of the Bessel function of the first kind J_0 .

I fit the intensity profiles to Eqn. 1.9 using different numbers of terms N . For the mCherry curves, the resulting fit parameters tended to converge as N increased, and the RMSE stabilized. However, neither was true for the NTF2 curves. Increasing values of N led to steadily decreasing values of diffusion constant. This may be due to the effect of binding on NTF2 diffusion.

1.4.2 Accumulation analysis

The total accumulation within the hydrogel can be modeled by integrating the concentration profile over the entire gel. When this is done, the averaged intensity within the hydrogel $N(t)$ is

Figure 1.8: Fits to Eqn. 1.8 near the beginning of the influx experiment for (A) mCherry and (B) NTF2-Alexa488 intensity profiles. Hydrogel nominally contains 10 mg/mL FSFG-PEGDA 700 kDa. The entire intensity profile is shown in the top panel with the portion used for fitting highlighted in red. Approximate locations of the gel edge, background fluorescence level, and partition coefficient are also shown.

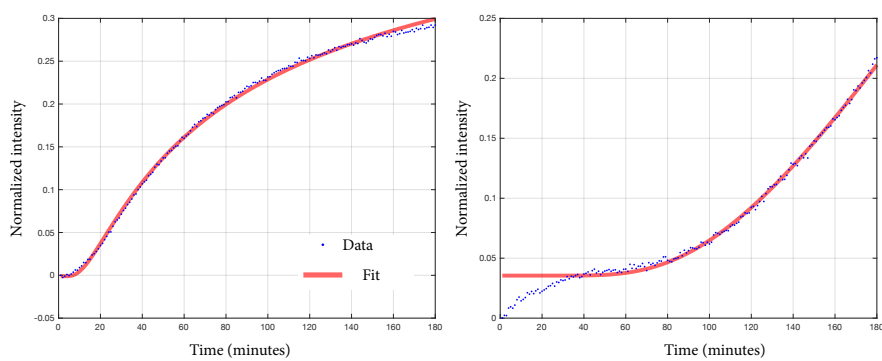
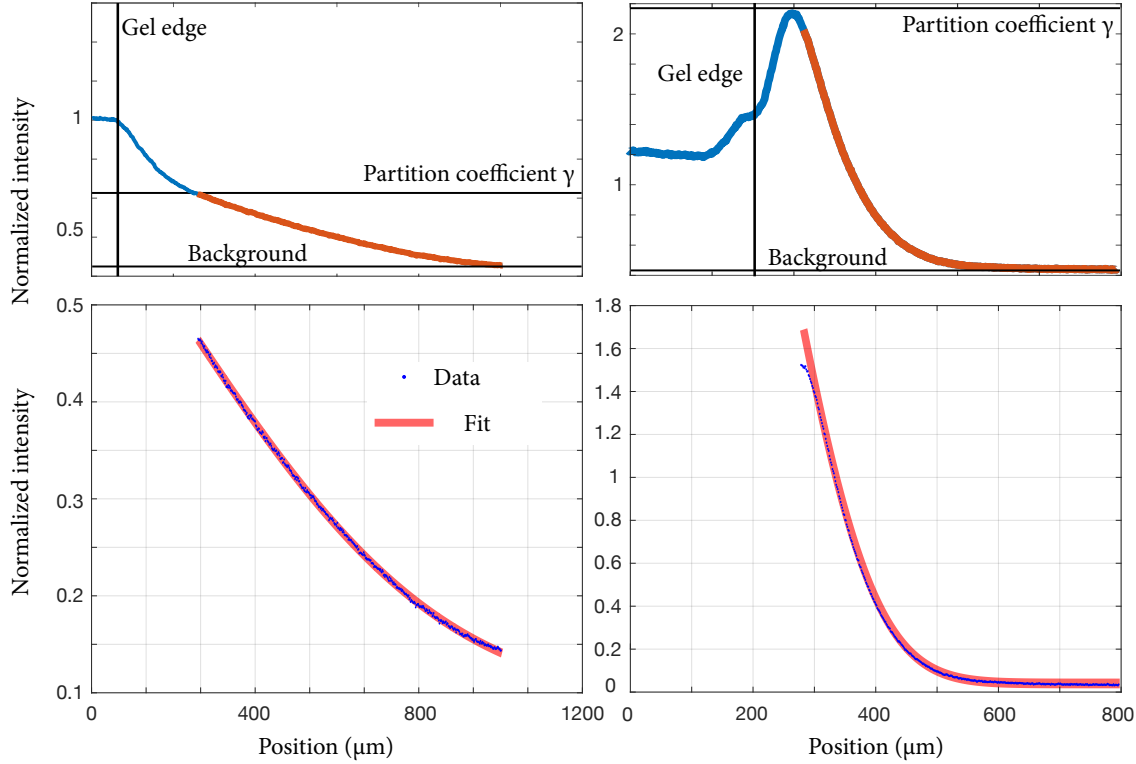


Figure 1.9: Fits to Eqn. 1.8 at a fixed point near the gel edge for (A) mCherry and (B) NTF2-Alexa488 intensity profiles. The short-time approximation likely only holds for times $t \lesssim 20$ minutes. Hydrogel nominally contains 10 mg/mL FSFG-PEGDA 700 kDa.

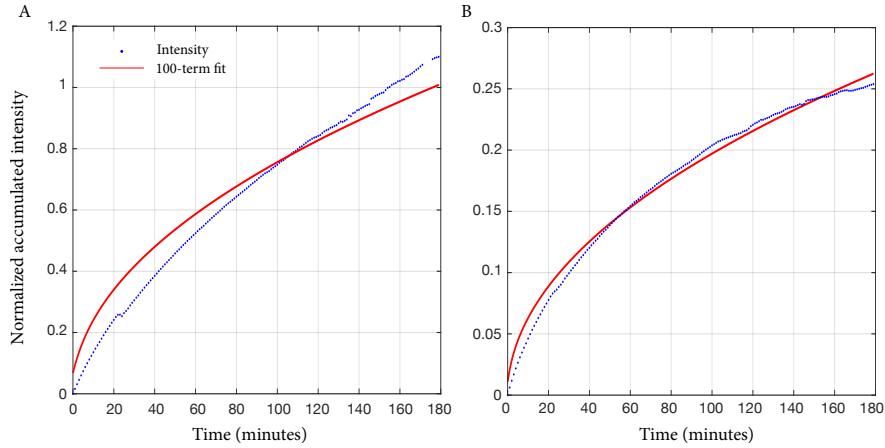


Figure 1.10: Accumulation fits to Eqn. 1.10 for (A) mCherry and (B) NTF2-Alexa488. Hydrogel nominally contains 10 mg/mL FSFG-PEGDA 700 kDa.

found to be

$$\frac{N(t)}{N_0} = 1 - \sum_{n=0}^{\infty} \frac{4}{(\alpha_n a)^2} \exp\left(-\frac{(\alpha_n a)^2 \pi t}{16\tau}\right) \quad (1.10)$$

where N_0 is the equilibrium value, here equal to the partition coefficient γ once the intensity has been normalized to that of the reservoir.

Fits to the first 100 terms of Eqn. 1.10 are shown in Fig. 1.10 for mCherry and NTF2. These fits had systematic error, likely for the same reasons as the profile fits.

While the profile and accumulation data do contain information on the diffusion constants of NTF2 and mCherry, I was unable to reliably extract that information using the influx experiments. The model presented above is a remarkably good match to the experimental setup except for the presence of binding and the unpredictable gel-edge effects. The FRAP experiments overcome the problem of edge effects by making use of equilibrated regions deep within the hydrogel.

1.5 FRAP analysis

1.5.1 Accounting for photobleaching

Small but noticeable amounts of photobleaching occur over the course of the FRAP experiment. In order to correct for photobleaching, the intensity of the bleached spot must be normalized to that of the entire gel, including the bleached region. The normalized intensity used to fit the

recovery curves is given by

$$N(t) = \frac{c_b(t)}{c_g(t)} \quad (1.11)$$

where the average intensity of the bleach spot is $c_b(t) = C_b(t)/A_b$. The total intensity within the bleach spot is $C_b(t)$ and A_b is the area of the spot as shown in Fig. 1.4. The average intensity of the entire gel $c_g(t)$ is defined similarly. Using this normalization removes the effects of photobleaching, as verified by simulating recovery data with various photobleaching rates.

1.5.2 No-exchange solution to diffusion equation

The simplest realistic model of fluorescence recovery assumes that the hydrogel is perfectly uniform and equilibrated, that the presence of the gel is unimportant, and that there is no exchange of fluorescent proteins between the hydrogel and the reservoir during the experiment. Upon making those assumptions, the recovery curve can be fit using a sum of two Bessel functions as described in [4,5]. The model used in [5] distinguishes between binding affinity regimes; NTF2-FSFG binding is sufficiently transient that it falls into the effective diffusion regime, allowing standard diffusion equations to be used without modification to calculate an effective diffusion constant as described in Sec. 1.3.3. The solution to fluorescence recovery with effective diffusion is given by

$$N(t) = A \exp(-\tau_D/2t) (I_0(\tau_D/2t) + I_1(\tau_D/2t)) + C \quad (1.12)$$

where the diffusion lifetime τ_D is related to the diffusion constant by $D = w^2/\tau_D$ if w is the bleach spot radius.

The amplitude A and offset C are related to the bleach depth (given by C) and final recovered value (given by $A + C$). Typical bleach depths were 5-10% of the initial intensity and tended to be smaller for mCherry than for NTF2. In principle, the final recovered value reflects the immobile fraction of fluorophore. If there is an immobile fraction, the bleached region will not recover to its initial value. Given the weak binding between NTF2 and FSFG, we do not expect an appreciable immobile fraction of either NTF2 or mCherry. For the most part, the hydrogels appear

to recover to their initial value. A few do not, for reasons that are unclear even after accounting for photobleaching.

The no-exchange model fits well to the larger hydrogels and those that are well-equilibrated. Many of the large gels, however, were not fully equilibrated even after a 24 hour incubation with the reservoir solution. The concentration within these gels will change over the course of the experiment as they continue to equilibrate. Smaller hydrogels were quicker to uniformly equilibrate; however, these gels are small enough that exchange of fluorescent proteins with the reservoir is important over the timescale of FRAP recovery. Both of these problems can be accounted for using a more thorough solution to the diffusion equation.

1.5.3 Fourier transform solution to diffusion equation

To account for exchange of fluorescent proteins with the reservoir, as well as for incomplete equilibration, some of the assumptions of the previous section must be relaxed. In particular, the assumption of radial symmetry must be abandoned. In order to incorporate angular as well as radial dependence, the solution must be written as a sum over Bessel function and cosine modes. While such a solution is cumbersome, it allows for an accurate description of the concentration throughout the hydrogel immediately post-bleach. Additionally, the boundary condition can be defined so as to allow exchange between the hydrogel and reservoir.

This analysis begins by numerically calculating the two-dimensional polar Fourier transform of the initial concentration distribution within the gel, decomposing it into a finite number of modes weighted by their contribution to the image. These mode coefficients are then used to create the equation to which the experimentally-measured recovery curve is fit. The fit parameters include the observed diffusion coefficients for NTF2 and mCherry, allowing the bound diffusion constant to be determined as described in Sec. 1.3.3.

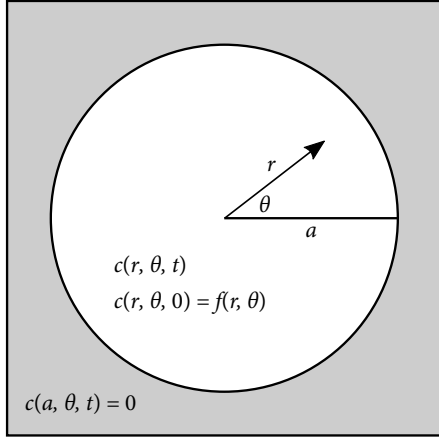


Figure 1.11: Geometry for diffusion-equation solution Eqn. 1.13. A circle of radius a is centered at the origin. The boundary $r = a$ is held at concentration $c = 0$ and the interior has initial concentration profile $f(r, \theta)$.

1.5.3.1 Analytic series solution

The problem is that of diffusion in a circular region of radius a , centered at the origin, whose boundary is held at a fixed concentration. The region $r < a$ has an arbitrary initial concentration distribution $f(r, \theta)$ which consists of the first post-bleach image (Fig. 1.11). To find the concentration $c(r, \theta, t)$ for $r < a$, we used the Green's function integrals described in [?], as heat transfer obeys the same differential equation as diffusion of particles. Green's functions describe a system's response to an instantaneous point source. An initial distribution can be built by integrating the Green's function over the region of interest. The correct Green's function must be identified for a particular geometry and set of boundary conditions, but a formal solution is straightforward to write once they have been obtained.

As this solution is two-dimensional, two sums must be taken over the basis functions. Bessel functions J_ν of the first kind and integer order ν are the radial basis, and cosines are the angular basis. The time dependence is carried by decaying exponentials whose time constant is related to the diffusion coefficient D as well as to the zeros of the Bessel functions. The terms are summed over the Bessel orders as well as over the zeros of each Bessel function. For our situation, the full

solution to the diffusion equation within the hydrogel is given by [?]

$$c(r, \theta, t) = \sum_{\nu=-\infty}^{\infty} \sum_{\alpha=0}^{\infty} \frac{\exp(-D\alpha^2 t) J_{\nu}(\alpha r)}{(J'_{\nu}(\alpha a))^2} \times b_{\nu, \alpha} \int_0^{2\pi} \int_0^a \cos(\nu(\theta - \theta')) J_{\nu}(\alpha r') f(r', \theta') r' dr' d\theta' \quad (1.13)$$

where, as in the previous section, αa are the zeros of J_{ν} , and $b_{\nu, \alpha}$ are normalization constants defined in Sec. 1.5.3.2. Note that the sums run over all positive and negative integer Bessel orders and over all zeros of each Bessel function.

This solution applies to a circle whose boundary is held at $c = 0$, so it must be shifted by an offset in order to match the experimental concentration at the boundary. Note that the relevant boundary concentration is just within the hydrogel, not the concentration of the reservoir. The reservoir is assumed to be infinite, in order to maintain the hydrogel edge at its equilibrium concentration, but the concentration of the reservoir itself is irrelevant.

The integral above is difficult to use as written because it contains both primed and unprimed coordinates in the angular term, $\cos(\nu(\theta - \theta'))$. The unprimed coordinate can be removed from the integral using the identity

$$\cos(\phi_1 - \phi_2) = \cos \phi_1 \cos \phi_2 + \sin \phi_1 \sin \phi_2$$

The mode coefficients $C_{\nu, \alpha}$ and $S_{\nu, \alpha}$ can then be defined as

$$c(r, \theta, t) = \sum_{\nu=-\infty}^{\infty} \sum_{\alpha=0}^{\infty} \frac{\exp(-D\alpha^2 t) J_{\nu}(\alpha r)}{(J'_{\nu}(\alpha a))^2} (C_{\nu, \alpha} \cos(\nu \theta) + S_{\nu, \alpha} \sin(\nu \theta)) \quad (1.14)$$

with

$$C_{n, \alpha} = b_{\nu, \alpha} \int_0^{2\pi} \int_0^a \cos(\nu \theta') J_{\nu}(\alpha r') f(r', \theta') r' dr' d\theta' \quad (1.15)$$

$$S_{n, \alpha} = b_{\nu, \alpha} \int_0^{2\pi} \int_0^a \sin(\nu \theta') J_{\nu}(\alpha r') f(r', \theta') r' dr' d\theta' \quad (1.16)$$

The problem is reduced to determining the mode coefficients by evaluating the integrals.

1.5.3.2 Calculating mode coefficients

Before mode coefficients can be calculated using Eqns. 1.15 and 1.16, the normalization constants $b_{\nu,\alpha}$ must be determined. To find an expression for them, begin with Eqn. 1.23 at $t = 0$, when $c(r, \theta, 0) = f(r, \theta)$.

$$f(r, \theta) = \sum_{\nu=-\infty}^{\infty} \sum_{\alpha=0}^{\infty} \frac{J_{\nu}(\alpha r)}{(J'_{\nu}(\alpha a))^2} (C_{\nu,\alpha} \cos(\nu\theta) + S_{\nu,\alpha} \sin(\nu\theta)) \quad (1.17)$$

This expression for $f(r, \theta)$ can be substituted into Eqns. 1.15 and 1.16. Using the cosine coefficients as an example,

$$\begin{aligned} C_{n,\alpha} &= b_{\nu,\alpha} \int_0^{2\pi} \int_0^a \cos(\nu\theta') J_{\nu}(\alpha r') \times \\ &\quad \left[\sum_{\mu=-\infty}^{\infty} \sum_{\beta=0}^{\infty} \frac{J_{\mu}(\beta r')}{(J'_{\mu}(\beta a))^2} (C_{\mu,\beta} \cos(\mu\theta') + S_{\mu,\beta} \sin(\mu\theta')) \right] r' dr' d\theta' \\ C_{n,\alpha} &= b_{\nu,\alpha} \sum_{\mu=-\infty}^{\infty} \sum_{\beta=0}^{\infty} \int_0^{2\pi} \int_0^a \cos(\nu\theta') \frac{J_{\nu}(\alpha r') J_{\mu}(\beta r')}{(J'_{\mu}(\beta a))^2} \times \\ &\quad (C_{\mu,\beta} \cos(\mu\theta') + S_{\mu,\beta} \sin(\mu\theta')) r' dr' d\theta' \\ C_{n,\alpha} &= b_{\nu,\alpha} \int_0^{2\pi} \int_0^a \frac{J_{\nu}^2(\alpha r')}{(J'_{\nu}(\alpha a))^2} (C_{\nu,\alpha} \cos^2(\nu\theta') + S_{\nu,\alpha} \cos(\nu\theta') \sin(\nu\theta')) r' dr' d\theta' \end{aligned}$$

The integral and sum have been switched and the orthogonality of the basis functions used to collapse the sums. The integral of the $S_{\nu,\alpha}$ term vanishes, as it is an odd function ($\cos(\nu\theta') \sin(\nu\theta')$) integrated over all θ' . Similarly, the $C_{\nu,\alpha}$ term drops from the sine coefficient integral. The remaining term gives

$$C_{n,\alpha} = b_{\nu,\alpha} \int_0^{2\pi} \int_0^a \frac{J_{\nu}^2(\alpha r')}{(J'_{\nu}(\alpha a))^2} C_{\nu,\alpha} \cos^2(\nu\theta') r' dr' d\theta'$$

or finally

$$\frac{1}{b_{\nu,\alpha}} = \int_0^{2\pi} \int_0^a \frac{J_{\nu}^2(\alpha r') \cos^2(\nu\theta')}{(J'_{\nu}(\alpha a))^2} r' dr' d\theta' \quad (1.18)$$

So long as the integral is truly over the entire circle $r < a$, this constant is the same for both $C_{\nu,\alpha}$ and $S_{\nu,\alpha}$. In that case, Eqn. 1.18 gives $b_{\nu,\alpha} = 2/\pi a^2$ for every mode.

However, in many cases, it is not possible to numerically integrate over the entire gel, as seen in Fig. 1.4D. All numerical integrals are instead over the gel mask, which encompasses as much of

the gel as fits into the field of view. The value of this mask is one within the gel and zero outside, so it serves to define the limits of numerical integration. Denoting the area covered by this mask as Ω , the normalization constants for $C_{\nu,\alpha}$ and $S_{\nu,\alpha}$, respectively, are

$$1/b_{\nu,\alpha}^C = \int_{\Omega} \frac{J_{\nu}^2(\alpha r') \cos^2(\nu\theta')}{(J'_{\nu}(\alpha a))^2} r' dr' d\theta' \quad (1.19)$$

$$1/b_{\nu,\alpha}^S = \int_{\Omega} \frac{J_{\nu}^2(\alpha r') \sin^2(\nu\theta')}{(J'_{\nu}(\alpha a))^2} r' dr' d\theta' \quad (1.20)$$

Likewise, the numerical integrals in Eqns. 1.15 and 1.16 are more precisely written

$$C_{n,\alpha} = b_{\nu,\alpha}^C \int_{\Omega} \cos(\nu\theta') J_{\nu}(\alpha r') f(r', \theta') r' dr' d\theta' \quad (1.21)$$

$$S_{n,\alpha} = b_{\nu,\alpha}^S \int_{\Omega} \sin(\nu\theta') J_{\nu}(\alpha r') f(r', \theta') r' dr' d\theta' \quad (1.22)$$

The degree to which the resulting coefficients deviate from the ideal case of a perfect circle can be roughly quantified by the ratio $b_{\nu,\alpha}/(2/\pi a^2) = \pi a^2 b_{\nu,\alpha}/2$. For small hydrogels, which entirely fit into the field of view, these values range from 1.01 to 1.03, signifying deviations of up to 3%. Large hydrogels whose top and bottom were cut from the field of view had deviations of up to 10%. However, using Eqns. 1.19 and 1.19 instead of the uniform mode weighting $b_{\nu,\alpha} = 2/\pi a^2$ should compensate for the irregular area of integration.

For every hydrogel, Bessel order ν , and Bessel zero α , mode coefficients were calculated numerically. The polar coordinates (r, θ) were converted to Cartesian (x, y) and a sum taken over all the pixels of the initial post-bleach image $f(x, y)$, using the hydrogel mask to set the limits. The center of the coordinate system was set at the center of the gel and the value of the gel radius a calculated as described in Sec. 1.3.1. Before the sum was calculated, the average intensity of the equilibrated portions of the hydrogel was subtracted from the entire image, effectively setting the equilibrium concentration at $c = 0$ as required by the series solution.

The sum was scaled using the area represented by each pixel (using the scale 1.58 $\mu\text{m}/\text{pixel}$) and normalized using the weighting constants $b_{\nu,\alpha}$. The final values of $C_{\nu,\alpha}$ and $S_{\nu,\alpha}$ were stored in two arrays for use in constructing the equation to which the experimental data was fit.

1.5.3.3 Reconstruction of initial image

To verify the mode coefficients, I reconstructed the initial post-bleach image from which they were calculated. The image was reconstructed by numerically integrating Eqn. 1.17 using a similar method to that discussed in the previous section. The area outside the gel mask was not reconstructed. Figure 1.12 shows the resulting reconstructions as the number of terms in the series increases. The relative magnitudes of those terms are plotted in Fig. 1.13. The reconstruction is adequate for our purposes by the time $N_\nu = 20$ and $N_\alpha = 20$, i.e. twenty Bessel orders and twenty zeros are used. Note that the Bessel orders are given by $\nu = -10, -9, \dots, 0, \dots, 8, 9$. A coefficient array of this size allowed a dataset of 43 hydrogels to be entirely processed and fit in approximately 24 hours on a desktop computer; larger coefficient arrays would require the use of a computing cluster.

1.5.3.4 Fitting recovery curves

Once the mode coefficients had been calculated, a fit string was constructed using the full series equation Eqn. 1.23 and fed into the Matlab curve fitter. Careful thought was required to ensure that the model was treated in the same way as the experimental data.

To begin, the mode coefficients were used to predict the average intensity of the bleach spot at each time point. Since the time dependence in each term is only in a decaying exponential, the average value of the bleach spot could be determined by integrating over the bleach spot:

$$\bar{c}_{\text{bleach}}(D, t) = \frac{1}{A_B} \sum_{\nu=-\infty}^{\infty} \sum_{\alpha=0}^{\infty} \exp(-D\alpha^2 t) \int_{\Omega_B} \frac{J_\nu(\alpha r)}{(J'_\nu(\alpha a))^2} (C_{\nu,\alpha} \cos(\nu\theta) + S_{\nu,\alpha} \sin(\nu\theta)) dA \quad (1.23)$$

where Ω_B is the region defined by the bleach-spot mask and A_B its total area. The Bessel function derivative J'_ν was computed using the identity

$$J'_\nu(x) = \frac{1}{2} (J_{\nu-1}(x) - J_{\nu+1}(x))$$

The average intensity of the entire gel, including the bleach spot, was determined in the same way, using the hydrogel mask instead of the bleach-spot mask. Both results were formatted as strings of sums, containing numerical values wherever possible as well as the diffusion constant parameter D (units of $\mu\text{m}^2/\text{s}$) and the time variable t , measured in seconds.

Figure 1.12: Reconstruction of initial concentration distribution. Reservoir is masked and not included. (A) Heatmap of original image with average equilibrated gel intensity set to zero. (B) Reconstruction using two Bessel orders ($N_\nu = 2$) and two zeros ($N_\alpha = 2$) in each order. (C-E) Reconstructions with $N_\nu = N_\alpha = 4, 10$, and 20 .

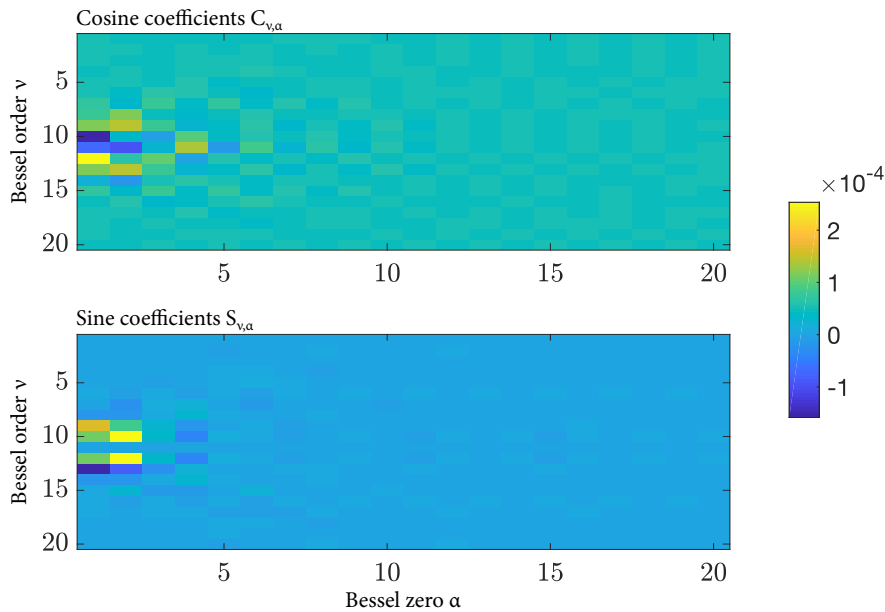
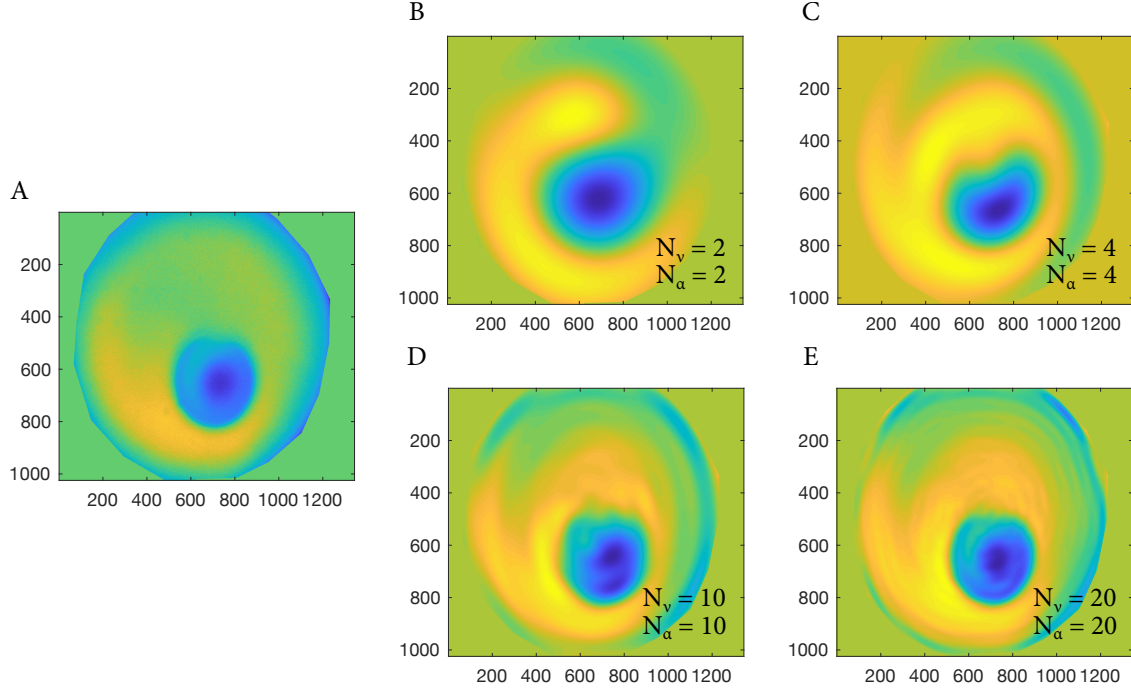
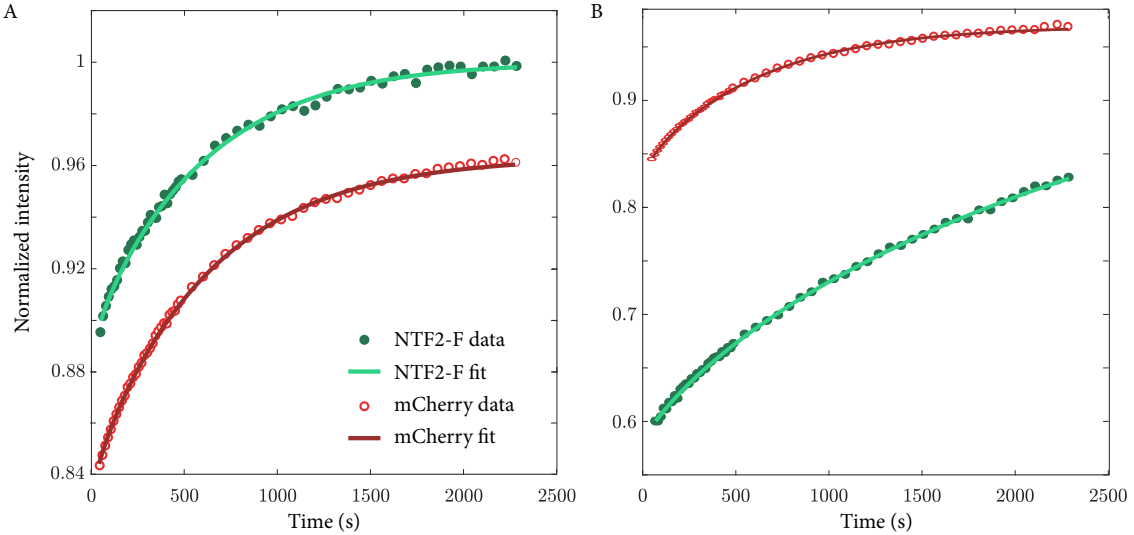


Figure 1.13: Heatmap of cosine and sine mode coefficients $C_{\nu,\alpha}$ and $S_{\nu,\alpha}$ for the reconstruction shown in Fig. 1.12E. Values are shown for each Bessel order ν and each zero α .

Figure 1.14: Fits using the series expansion Eqn. 1.13. (A) NTF2-F and mCherry recovery curves for a no-nup hydrogel. (B) NTF2-F and mCherry recovery curves for a hydrogel nominally containing 10 mg/mL FSFG concat-1.



Once these strings were created, the equilibrium concentration value c_0 was added back to both of them, and their ratio was taken, in order to mimic the data processing in Sec. 1.5.1. Mathematically, this gave a normalized string of

$$f(D, t) = \frac{\bar{c}_{\text{bleach}}(D, t) + c_0}{\bar{c}_{\text{gel}}(D, t) + c_0} \quad (1.24)$$

At this point, I checked the normalization by simulating data using the value of D calculated from the no-exchange analysis in Sec. 1.5.2. Often the simulated data matched the experiment to within 10%, but further fit parameters were needed in order to fit the data well. Ultimately, the function to which the data were fit was

$$g(c_1, c_2, D, t) = c_1 f(D, t) + c_2 \quad (1.25)$$

where c_1 and c_2 reflect the bleach depth and final recovered concentration similarly to A and C in Sec. 1.5.2. Their values are less important than that of the diffusion constant D .

Fits such as those shown in Fig. 1.14 were typical results. Values for c_1 and c_2 were of order unity, except for a few fits that were clearly incorrect and were omitted from the final dataset.

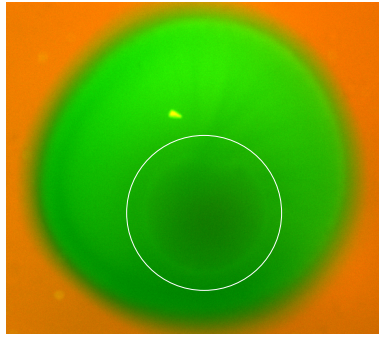


Figure 1.15: Bright NTF2-F ring surrounding photobleach spot, 70 minutes after bleaching. This ring often developed in FSFG concat-1 gels. Photo-bleach mask was chosen to be slightly smaller than the ring. Contrast adjusted for ease of viewing. While circle added to guide the eye.

1.6 Results

In all, FRAP analysis was performed on 36 hydrogels: 15 no-nup gels, 12 nominally containing 10 mg/mL FSFG concat-1, and 10 containing FSFG concat-2. (lookup: double-check the ones with low concentration) Of the FSFG concat-2 hydrogels, seven had a nominal concentration of 20 mg/mL FSFG concat-2, meaning that in principle they had the same molar concentration as the FSFG concat-1 gels, but twice as many FG repeats. The other three nominally contained 10 mg/mL FSFG concat-2, giving them half as many chains but the same number of FG repeats as the FSFG concat-1 gels. The mean partition coefficients and diffusion constants were not significantly different between the two groups of FSFG concat-2 gels and they were treated as one condition in the following results.

Many of the FSFG concat-1 hydrogels showed an unusual bright ring in the NTF2-F channel around the photobleach spot which developed slowly after bleaching. Figure 1.15 shows an example. The ring is presumably due to photodamage by bleaching, but it is not clear why the edge of the bleach spot would exhibit increased NTF2-F binding. When hydrogels showed this bright ring, care was taken when drawing the bleach spot mask to exclude the ring entirely.

The partition coefficients for NTF2-F and mCherry are shown in Fig. 1.16 along with the corresponding fraction bound. As expected, the partition coefficients NTF2-F and mCherry are very similar in the no-nup hydrogels, while the NTF2-F partition coefficient increases for FSFG hydrogels due to binding. The FSFG concat-2 hydrogels show the highest NTF2-F partition coefficient, likely because there are more FG repeats in total. The fraction bound follows similar trends, although

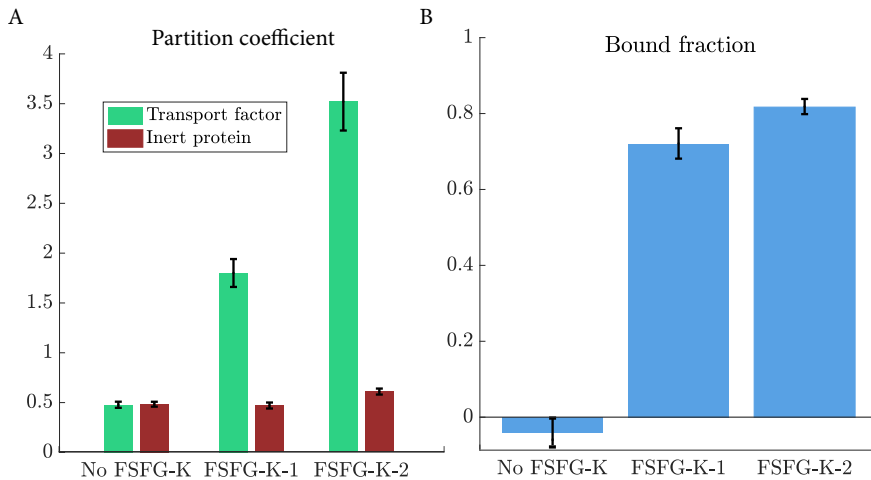


Figure 1.16: (A) Partition coefficients for NTF2-F and mCherry in each of the three experimental conditions. (B) Fraction of NTF2-F bound as calculated using Sec. 1.3.2. All errors are standard error of the mean.

the difference between the FSFG concat-1 and concat-2 hydrogels is less pronounced. The fraction of NTF2-F bound to the no-nup hydrogels is indistinguishable from zero.

Figure 1.17 shows normalized recovery curves for all hydrogels in the dataset. In addition to the normalization described in Sec. 1.5.1, these curves were also scaled so that the pre-bleach average bleach spot intensity was one. Dark curves show the average NTF2 and mCherry recovery curves for each condition. The most obvious difference between conditions is the greater bleach depth for NTF2-F in FSFG hydrogels. Bleach depth stays roughly constant for mCherry between conditions.

Finally, the observed diffusion constants for NTF2-F and mCherry were calculated using the Fourier series model. Mean values for each of the experimental conditions are shown in Fig. A.4 along with calculated bound diffusion constants. The observed diffusion for NTF2-F and mCherry was roughly equal in the no-nup hydrogels, but NTF2-F has a much lower diffusion constant in the FSFG conditions, due to binding. Two-tailed t-tests were conducted with the null hypothesis that $D_B = 0$. For FSFG concat-1, the resulting p-value was $p = 0.025$; for FSFG concat-2, it was $p = 0.083$. There is no distinguishable difference between D_B for FSFG concat-1 and FSFG concat-2, which may be due to the lack of sensitivity in our measurements.

Figure 1.17: Recovery curves for (A) no-nup, (B) FSFG concat-1, and (C) FSFG concat-2 hydrogels. All curves are shown for both NTF2-F and mCherry. Dark lines are averaged curves. Pre-bleach intensity set to one.

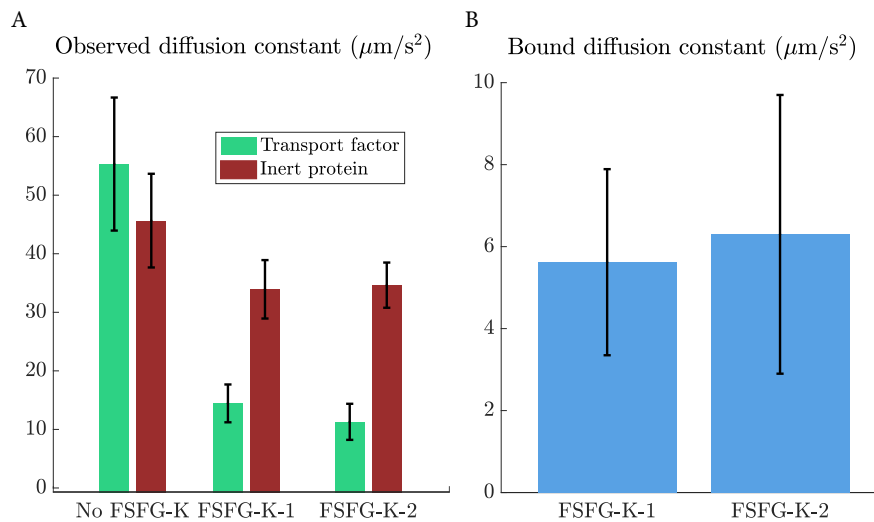
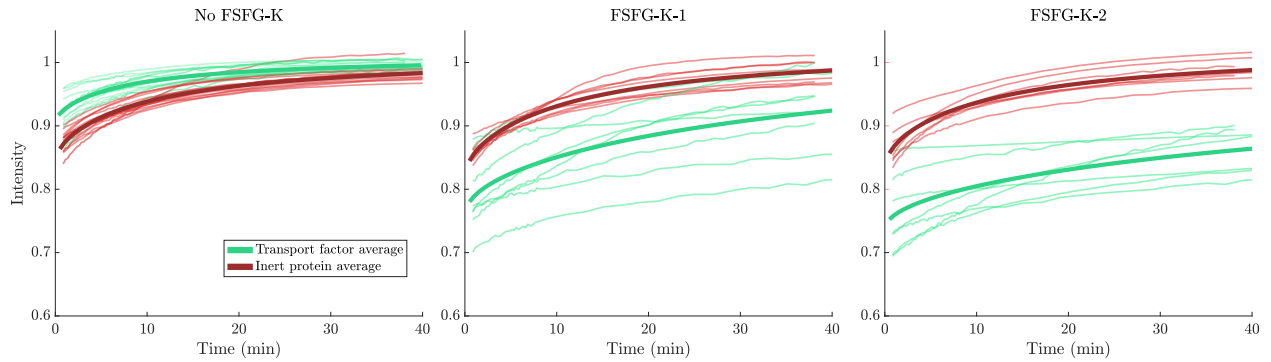


Figure 1.18: (A) Observed diffusion constant for NTF2-F and mCherry in each of the three experimental conditions. (B) Calculated values of the bound diffusion constant D_B for NTF2-F in the FSFG hydrogels. All errors shown are standard error of the mean.

1.7 Discussion

Our goal was to create a material in which we could measure and test the properties of bound diffusion. These results suggest that we can indeed measure non-zero bound diffusion, although there is no statistically significant difference between Nups of different lengths and valencies. Smaller effects would be measurable if the fraction of transport factor bound (p_B) increased, as then the contribution of bound diffusion to the observed diffusion would become more prominent. The most straightforward way of increasing the fraction bound is to increase the concentration of tethered Nups within the gel, a task which has proven difficult. However, this dataset still provides a check on the predictions of our model.

Our bound-state diffusion model can predict the values of bound diffusion constant D_B that we expect to observe, provided we input an estimate of the off-rate k_{off} and assume that tethered diffusion the only mechanism of bound-state mobility (Appendix A). Taking $K_D \approx 0.5$ mM for FSFG concat-1 and $K_D \approx 0.4$ mM for FSFG concat-2, we can predict D_B for each FSFG hydrogel [1]. For FSFG concat-1 hydrogels, the predicted bound diffusion constant is $D_B = 6.9 \pm 0.3$ $\mu\text{m}^2/\text{s}$; for FSFG concat-2 gels this value is $D_B = 9.3 \pm 0.3$ $\mu\text{m}^2/\text{s}$. These values are consistent with our measured mean values of $D_B = 5.6 \pm 2.3$ $\mu\text{m}^2/\text{s}$ for FSFG concat-1 gels and $D_B = 6.3 \pm 3.4$ $\mu\text{m}^2/\text{s}$ for FSFG concat-2 gels. However, the large standard error in our measurements suggests that better measurements are needed before we can strongly state that our model has accurately predicted the bound diffusion constant.

The hydrogel nuclear pore mimics discussed in this chapter do not reproduce the selectivity properties of nuclear transport; the tethered Nup concentration is too low and the transport factor - Nup dissociation constant is too high. However, they do provide a platform from which to measure bound diffusion. Non-zero bound diffusion of transport factors was measured when Nups were tethered to the hydrogel. This represents a first step towards understanding the effect of bound diffusion on selective biofilters.

Bibliography

- [1] R. Hayama, S. Sparks, L. M. Hecht, K. Dutta, J. M. Karp, C. M. Cabana, M. P. Rout, and D. Cowburn. Thermodynamic characterization of the multivalent interactions underlying rapid and selective translocation through the nuclear pore complex. *Journal of Biological Chemistry*, 293(12):4555–4563, March 2018.
- [2] S. Milles, D. Mercadante, I. V. Aramburu, M. R. Jensen, N. Banterle, C. Koehler, S. Tyagi, J. Clarke, S. L. Shammas, M. Blackledge, F. Gräter, and E. A. Lemke. Plasticity of an Ultra-fast Interaction between Nucleoporins and Nuclear Transport Receptors. *Cell*, 163(3):734–745, October 2015.
- [3] N. A. Mortensen, F. Okkels, and H. Bruus. Universality in edge-source diffusion dynamics. *Physical Review E*, 73(1), January 2006.
- [4] Y. J. Yang, D. J. Mai, T. J. Dursch, and B. D. Olsen. Nucleopore-Inspired Polymer Hydrogels for Selective Biomolecular Transport. *Biomacromolecules*, September 2018.
- [5] B. L. Sprague, R. L. Pego, D. A. Stavreva, and J. G. McNally. Analysis of Binding Reactions by Fluorescence Recovery after Photobleaching. *Biophysical Journal*, 86(6):3473–3495, June 2004.

Appendix A

Hydrogel nuclear pore mimic dataset

This appendix gives the parameters calculated for each hydrogel in the FRAP dataset, organized by FSFG condition. The predicted values for bound diffusion constant D_B and bound to free diffusion ratio D_B/D_F assume that the only mechanism of bound diffusion is tethered diffusion, so that

$$\frac{D_B}{D_F} = \frac{L_c \ell_p k_{\text{off}}}{L_c \ell_p k_{\text{off}} + 3D_F}$$

The parameters used are given in Fig. A.1. The K_D values are average values from [1]. The on-rate k_{on} is assumed to be diffusion-limited. Diffusion constants have units of $\mu\text{m}^2/\text{s}$. Partition coefficients (γ) and fraction of NTF2 bound (p_B) are unitless.

	FSFG concat-1	FSFG concat-2
L_c (aa)	124	248
L_c (m)	4.96E-08	9.92E-08
Length per aa (m)	4.00E-10	4.00E-10
ℓ_p (m)	1.00E-09	1.00E-09
K_D (M)	0.000545	0.000395
k_{on} ($\text{M}^{-1} \text{s}^{-1}$)	1.00E+09	1.00E+09
k_{off} (s^{-1})	5.45E+05	3.95E+05

Figure A.1: Parameters used to predict the bound diffusion constant for NTF2-F in FSFG hydrogels. Binding data is from [1].

Figure A.2: Measured and calculated values for no-Nup hydrogels.

	Dataset index	Experiment ID	D _{obs} NTF2	D _{obs} mCherry	γ NTF2	γ mCherry	p _B
	1	'19-1-3_1'	41.6	26.7	0.64	0.52	0.19
	4	'19-2-6_1'	68.7	71.2	0.57	0.52	0.10
	7	'19-2-6_7'	25.3	26.4	0.52	0.52	-0.01
	10	'19-2-6_13'	177.3	126.3	0.60	0.69	-0.16
	13	'19-2-6_19'	72.0	71.5	0.66	0.61	0.07
	18	'19-2-12_7'	33.1	25.8	0.44	0.47	-0.08
	20	'19-2-12_11'	100.1	68.1	0.42	0.49	-0.16
	24	'19-2-15_1'	26.8	26.5	0.21	0.30	-0.45
	25	'19-2-15_7'	31.2	27.6	0.40	0.42	-0.05
	26	'19-2-15_13'	74.8	61.4	0.48	0.45	0.06
	28	'19-2-15_19'	10.9	15.2	0.42	0.42	-0.01
	30	'19-2-19_1'	37.8	32.0	0.53	0.52	0.02
	31	'19-2-19_7'	18.3	15.6	0.39	0.42	-0.07
	33	'19-2-19_19'	40.8	44.2	0.44	0.41	0.06
	41	'19-2-21_19'	82.9	57.9	0.45	0.47	-0.04
Mean			56.10	46.44	0.48	0.48	-0.04
Standard deviation			42.52	29.94	0.11	0.09	0.15
Standard error of the mean			11.36	8.00	0.03	0.02	0.04

Figure A.3: Measured and calculated values for FSFG concat-1 hydrogels, nominally containing 10 mg/mL FSFG.

	Dataset index	Experiment ID	D _{obs} NTF2	D _{obs} mCherry	γ NTF2	γ mCherry	p _B	D _B	using ITC data	Predicted D _{B/D_F}	Predicted D _B
	2	'19-1-3_3'	29.0	49.1	2.06	0.54	0.74	21.84	0.16	7.61	
	5	'19-2-6_3'	7.2	41.9	1.89	0.46	0.76	-3.91	0.18	7.41	
	8	'19-2-6_9'	13.9	22.9	1.31	0.54	0.59	7.71	0.28	6.47	
	11	'19-2-6_15'	13.4	36.1	1.53	0.42	0.72	4.76	0.20	7.21	
	14	'19-2-6_21'	20.2	46.0	1.77	0.41	0.77	12.48	0.16	7.54	
	16	'19-2-12_3'	12.5	22.3	1.77	0.56	0.69	7.95	0.29	6.42	
	19	'19-2-12_9'	10.9	41.4	1.63	0.47	0.71	-1.51	0.18	7.40	
	21	'19-2-12_13'	42.4	70.4	1.03	0.63	0.38	-2.78	0.11	7.99	
	27	'19-2-15_15'	10.0	19.4	1.65	0.36	0.78	7.41	0.32	6.16	
	32	'19-2-19_15'	4.8	35.9	2.20	0.39	0.82	-1.82	0.20	7.20	
	34	'19-2-19_21'	7.4	20.2	1.84	0.36	0.81	4.28	0.31	6.23	
	39	'19-2-21_15'	11.0	10.9	2.95	0.46	0.84	10.96	0.45	4.93	
Mean			15.23	34.71	1.80	0.47	0.72	5.62	0.24	6.88	
Standard deviation			10.71	16.55	0.48	0.09	0.13	7.52	0.10	0.86	
Standard error of the mean			3.23	4.99	0.14	0.03	0.04	2.27	0.03	0.26	

Figure A.4: Measured and calculated values for FSFG concat-2 hydrogels.

	Dataset index	Experiment ID	D _{obs} NTF2	D _{obs} mCherry	γ NTF2	γ mCherry	p _B	D _B	using ITC data	
									Predicted D _{B/D_F}	Predicted D _B
	6	'19-2-6_5'	12.78184	44.56024563	3.23	0.70	0.78	4.04	0.23	10.10
	9	'19-2-6_11'	10.307	43.18354162	2.82	0.66	0.77	0.24	0.23	10.03
	12	'19-2-6_17'	8.353138	30.91040114	3.24	0.50	0.85	4.22	0.30	9.18
	17	'19-2-12_5'	9.398679	42.56939841	4.41	0.67	0.85	3.49	0.23	9.99
	22	'19-2-12_15'	26.73285	39.71193071	2.64	0.68	0.74	22.25	0.25	9.83
	23	'19-2-12_17'	16.29925	53.36041486	2.89	0.73	0.75	3.88	0.20	10.49
	35	'19-2-19_23'	5.88424	34.98831302	2.78	0.57	0.80	-1.54	0.27	9.51
	37	'19-2-21_11'	27.91552	29.00498627	3.49	0.41	0.88	27.77	0.31	9.01
	40	'19-2-21_17'	2.634705	18.14683742	4.72	0.55	0.88	0.61	0.42	7.59
	43	'19-2-21_23'	0.534426	17.81107527	5.02	0.63	0.87	-1.95	0.42	7.54
Mean			12.08	35.42	3.52	0.61	0.82	6.30	0.29	9.33
Standard deviation			9.24	11.57	0.87	0.10	0.06	10.20	0.08	1.03
Standard error of the mean			3.08	3.86	0.29	0.03	0.02	3.40	0.03	0.34